

An Efficient Approach into Finite Element Method for Lateral Buckling Analysis of Fiber-Metal Laminates Tapered I-Beams

Masoumeh Soltani^{1*}, Azadeh Soltani¹

¹ Department of Civil Engineering, Faculty of Engineering, University of Kashan, Isfahan Province, Qotb-e Ravandi Blvd, 8731753153 Kashan, Iran

* Corresponding author, e-mail: msoltani@kashanu.ac.ir

Received: 22 July 2021, Accepted: 03 May 2022, Published online: 08 June 2022

Abstract

In this paper, lateral stability analysis of fiber-metal laminated (FML) doubly-symmetric tapered I-beams with symmetrical lay-up for all section walls is perused by presenting a new finite element solution. Vlasov's thin-walled beam theory is utilized to consider the bending–twisting coupling effect. Based on the classical lamination theory as well as the energy method, the total potential energy is derived for the flexural displacements and the twist angle. Using an auxiliary function, the variational formulation is then constructed only in terms of the twist angle. To precisely determine 4*4 elastic and buckling stiffness matrices, Hermitian cubic polynomial is applied as the shape functions into the resulting variational statement. The most beneficial feature of the present finite element model is to provide a two-node laminated I-beam element with a low number of degrees of freedom. Lateral buckling strength of thin-walled FML profile having varying I-section has been calculated for E-glass/epoxy as composite and aluminum as metal. The obtained results are compared with finite element solutions using ANSYS software and showed excellent agreement with them. Also, the effects of different consequential parameters such as fiber orientation, lay-up sequence, metal volume fraction, web tapering ratio, and transverse load height position on lateral stability resistance of fixed-free FML tapered I-beams subjected to uniformly distributed load are comprehensively investigated.

Keywords

fiber metal laminates, tapered thin-walled beam, lateral-torsional stability, finite element formulation

1 Introduction

The use of thin-walled structural components in the most innovative engineering fields including aircraft wings, turbine blades, steel frames and decks of bridge has become increasingly common throughout the years. Although thin-walled open cross-sections have some features such as high ratios of stiffness-to-weight and strength-to-weight, they have some drawbacks such as local buckling, poor torsion rigidity and low out-of-plane bending resistance. As a result of these disadvantages, a laterally unbraced thin-walled beam subjected to bending about its strong axis may buckle in a flexural–torsional mode. Hence, this situation results in a lower stability strength. Moreover, in recent years, the thin-walled beams with variable cross-section have been extensively adopted in aeronautical, mechanical, and civil engineering applications due to the importance of having an optimum distribution of weight and strength. With the development of fabrication processes specifically pultrusion, the use of

thin-walled structural components made up of fiber-reinforced composite materials in aeronautical and mechanical installations has become increasingly common throughout the years. The main reason for this increase is the desirable features of composites, such as high fatigue resistance, durability, corrosion resistance, and optimization of structural weight. Engineers can produce structural components with favorable mechanical responses and enduring buckling resistance by using innovative materials. Fiber metal laminations (FMLs) are a new class of hybrid materials that are built from several thin sheets of metal alloys and fiber-reinforced epoxy composite plies. These laminates simultaneously possess the desirable features of metal such as ductility, damage tolerance, excellent resistance to impact and environmental conditions, as well as advantages of the reinforced polymeric composite. Due to the conspicuous characteristics of FMLs, the use of fiber-metal hybrid composite structures in the design of

submarine and aircraft industries has become increasingly common throughout the years. A review in the literature displays that several investigations have been conducted by different research to peruse the mechanical responses of laminated composite structural components. In the following, a short description of a few of those is presented.

Nam et al. [1] used a genetic algorithm to optimize the arrangement of metal-fiber multilayer composite shells under different loading cases. They indicated that metal-fiber multilayer shells made of carbon fiber-reinforced polymer laminates are more resistant to random and unforeseen forces in most loading conditions. Andrade et al. [2, 3] presented some useful works about the lateral-torsional stability analysis of thin-walled beams with doubly and singly symmetric I-section under different boundary conditions. Taking into account small deformations and large displacements, Mohri et al. [4] analyzed the lateral-torsional stability strength of thin-walled beams under transverse-axial loadings employing Galerkin's method. Ravishankar et al. [5] reported the influence of type fiber-reinforced epoxy composite materials, Metal Volume Fraction (MVF), and angular velocity on the free vibrational response of rotating beams made of FMLs and or functionally graded materials using finite element software. In addition, the mechanical response of laminated composite thin-walled members with uniform cross-section subjected to different loading cases and end conditions was completely studied in [6–16]. Using the finite difference method, Secer and Uzun [17] performed the inelastic ultimate load analysis of steel frames subjected to transverse distributed loads was performed by considering the lateral-torsional buckling effect in the load increment steps. Ghasemi and Mohandes [18, 19] and Ghasemi et al. [20] presented some useful works about analysis fiber-metal laminate (FML) cylindrical shells under different boundary conditions. Within the context of first-order shear deformation theory, a novel finite element technique was recently introduced by Ton-That and Nguyen-Van [21] to investigate the mechanical behavior of laminated plate and shell.

A literature review indicates that the vibration and buckling responses of prismatic laminated composited thin-walled members have been performed by a large number of authors, whereas the lateral stability analysis of the same structure with varying cross-section is not studied a lot. Due to the application of laminated composite thin-walled beams in civil and architecture industries, aircraft and spacecraft structures and the blades of wind turbines, there is a general lack of studies focusing on the lateral buckling

analysis of transversely loaded tapered sandwich composite thin-walled beams. Based on these facts, an efficient finite element model is developed for linear lateral stability analysis of hybrid fiber-metal laminates sandwich web and/or flanges tapered I-beams. The present finite element model is inspired by the two-noded 4degree-of-freedom element, recently introduced by Soltani et al. [22] for the lateral buckling analysis of non-prismatic thin-walled beams with axially varying materials. The main advantage of the new approach is facilitating lateral stability analysis of tapered thin-walled FML I-beams due to the application of the proposed element with a low number of degrees of freedom. The above task is performed, through the following stages:

In Section 2, based on the classical lamination theory assumption and Vlasov's model for thin-walled cross-sections, the total potential energy for the tapered thin-walled balanced laminated beam with I-section is firstly derived within the framework of elastic behavior. It is assumed that all section walls (the web and both flanges) are composed of two metal layers at the outer sides of the fiber-reinforced polymer laminates and laminated symmetrically concerning its mid-plane. Considering the flexural-twist coupling effects, the expression of potential energy is obtained in terms of the lateral deflection and the angle of twist. Following the method presented by Soltani et al. [22], Asgarian et al. [23] and Soltani et al. [24], the variational statement is finally derived only in terms of the twist angle. In Section 3, the elements of structural stiffness matrices, including elastic and buckling ones, are then determined using the expressions of the cubic Hermitian shape functions. Eventually, the lateral buckling loads can be calculated by solving the eigenvalue problem. This methodology is capable of precise estimation of the lateral buckling strength of laminated composite I-section beams with different types of variation in geometric features along the longitudinal direction and subjected to different end conditions and loading cases. Finally, an exhaustive illustrative example is performed to assess the influence of noticeable parameters such as metal volume fraction, fiber angle, lay-up arrangement, load height parameter and tapering ratio on the lateral stability resistance of FML I-shaped beam with variable cross-section. Lastly, the best probable lay-up is chosen to enhance the endurable lateral-torsional buckling load. One of the available commercial FMLs is GLARE (glass reinforced aluminum laminate), which is considered in this study. GLARE has good resistance to moisture and corrosion, high tensile and compressive strength, high failure strain, low weight, as well as good adhesion between glass fiber and resin.

2 Variational formulations

A schematic of thin-walled FML beam with of length L varying I-section subjected to uniformly distributed load is shown in Fig. 1. The orthogonal right-hand Cartesian coordinate system (x, y, z) is adopted, wherein x denotes the longitudinal axis and y and z are the first and second principal bending axes parallel to the flanges and web, respectively. The origin of these axes (O) is located at the centroid of the cross-section. As presented in Fig. 1, all section walls of the considered tapered bam consist of two metal sheets at the outer sides of fiber reinforced epoxy composite layers. Based on small displacements assumption and Vlasov's thin-walled beam theory for non-uniform torsion, the displacement fields can be expressed as [25]:

$$\begin{aligned}
 U(x, y, z) &= u_0(x) - y \frac{dv(x)}{dx} - z \frac{dw(x)}{dx} - \omega(y, z) \frac{d\theta(x)}{dx}, \\
 V(x, y, z) &= v(x) - z\theta(x), \\
 W(x, y, z) &= w(x) + y\theta(x).
 \end{aligned}
 \tag{1}$$

In these equations, U is the axial displacement and displacement components V and W represent lateral and vertical displacements (in direction y and z). The term $\omega(y, z)$

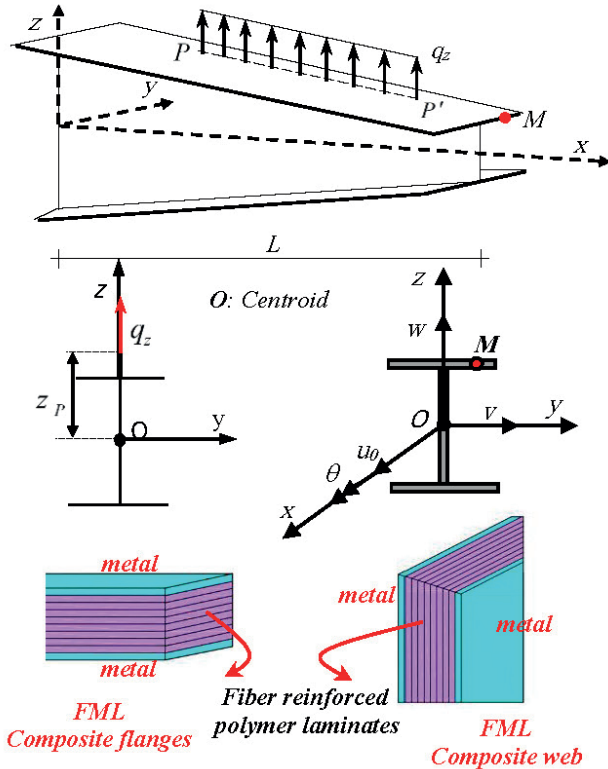


Fig. 1 FML beam with variable doubly symmetric I-section under external distributed loads: Coordinate system, notation for displacement parameters, definition of load eccentricities, and web and flanges lay-up arrangement

signifies a cross-section variable that is called the warping function, which can be defined based on Saint-Venant's torsion theory and θ is twisting angle.

Using the displacement field given in Eq. (1) and taking into account for tapering, the non-zero constituents of linear and non-linear parts of strain-displacement are respectively expressed as [12]

$$\begin{aligned}
 \varepsilon'_{xx} &= \frac{\partial U}{\partial x} = u'_0 - yv'' - zw'' - \omega\theta'', \\
 \varepsilon'_{yy} &= \frac{1}{2} \left(\frac{\partial U}{\partial y} + \frac{\partial V}{\partial x} \right) = -\frac{1}{2} \left(z + \frac{\partial \omega}{\partial y} \right) \theta', \\
 \varepsilon'_{zz} &= \left(\frac{\partial U}{\partial z} + \frac{\partial W}{\partial x} \right) = \frac{1}{2} \left(y - \frac{\partial \omega}{\partial z} \right) \theta', \\
 \varepsilon^*_{xx} &= \frac{1}{2} \left(\left(\frac{\partial V}{\partial x} \right)^2 + \left(\frac{\partial W}{\partial x} \right)^2 \right) = \frac{1}{2} [v'^2 + w'^2 + r^2\theta'^2] \\
 &\quad + yw'\theta' - zv'\theta', \\
 \varepsilon^*_{yy} &= \frac{1}{2} \left(\frac{\partial V}{\partial x} \frac{\partial V}{\partial y} + \frac{\partial W}{\partial x} \frac{\partial W}{\partial y} \right) = \frac{1}{2} (w' + \theta'y)\theta, \\
 \varepsilon^*_{zz} &= \frac{1}{2} \left(\frac{\partial V}{\partial x} \frac{\partial V}{\partial z} + \frac{\partial W}{\partial x} \frac{\partial W}{\partial z} \right) = -\frac{1}{2} (v' + \theta'z)\theta,
 \end{aligned}
 \tag{2}$$

where ε'_{ij} and ε^*_{ij} are dedicated to denotes the linear parts and the quadratic non-linear ones, respectively. In addition, the term r^2 in Eq. (3) represents $y^2 + z^2$.

Here, the variational statement of equilibrium equations is derived as

$$\delta\Pi = \delta U_l + \delta U_0 - \delta W_e = 0.
 \tag{4}$$

In this formulation, δ denotes a variational operator. U_l and U_0 represent the elastic strain energy and the strain energy due to effects of the initial stresses, respectively. W_e denotes work done by external applied loads. δU_l could be computed using the following equation.

$$\begin{aligned}
 \delta U_l &= \int_V \sigma_{ij} \delta \varepsilon'_{ij} dV = \int_0^L \int_A \sigma_{xx} \delta \varepsilon'_{xx} dA dx \\
 &\quad + 2 \int_0^L \int_A \sigma_{yy} \delta \varepsilon'_{yy} dA dx + 2 \int_0^L \int_A \sigma_{zz} \delta \varepsilon'_{zz} dA dx,
 \end{aligned}
 \tag{5}$$

in which, L expresses the element length. $\delta \varepsilon'_{ij}$ is the variation of the linear parts of strain tensor. Substituting the variation of the linear part of strain tensor components Eq. (2) into relation Eq. (5) yields:

$$\begin{aligned}
 \delta U_l &= \int_0^L \int_A \sigma_{xx} (\delta u'_0 - y\delta v'' - z\delta w'' - \omega\delta\theta'') dA dx \\
 &\quad + \int_0^L \int_A \sigma_{yy} \left(-\left(z + \frac{\partial \omega}{\partial y} \right) \delta\theta' \right) dA dx + \int_0^L \int_A \sigma_{zz} \left(\left(y - \frac{\partial \omega}{\partial z} \right) \delta\theta' \right) dA dx
 \end{aligned}
 \tag{6}$$

The expression of the elastic strain energy variation can be formulated in terms of section forces acting on cross-sectional contour of the elastic member in the buckled configuration. The resultants of classical stresses for beams with doubly-symmetric I-section can be expressed as follows [6, 7].

$$\begin{aligned} (N, M_y, M_z, B_\omega) &= \int_A \sigma_{xx}(1, z, -y, -\omega) dA, \\ M_{sv} &= \int_A \left(\sigma_{xz} \left(y - \frac{\partial \omega}{\partial z} \right) - \sigma_{xy} \left(z + \frac{\partial \omega}{\partial y} \right) \right) dA, \end{aligned} \quad (7)$$

where N is the axial force. M_y and M_z denote the bending moments about major and minor axes, respectively. B_ω is the bi-moment. M_{sv} is the St-Venant torsion moment. In this stage, by integrating Eq. (6) over the cross-section area of the beam and using relations Eq. (7), the variation form of the elastic strain energy is acquired as [24]:

$$\begin{aligned} \delta U_l &= \int_L (N \delta u'_0 + M_z \delta v'' - M_y \delta w'' + B_\omega \delta \theta'') dx \\ &+ \int_0^L (M_{sv} \delta \theta') dx. \end{aligned} \quad (8)$$

The present model is applied in the case of balanced and symmetrical lay-ups of the web and both flanges. In the context of classical laminated plate theory and substitution the expressions of linear strain tensor (ϵ_{ij}^l) presented in Eq. (2) into Eq. (7), the stress resultants of symmetrically balanced laminates are derived in terms of displacement components as [12]

$$\begin{aligned} N &= (EA)_{com} u'_0, \\ M_z &= (EI_z)_{com} v'', \quad M_y = -(EI_y)_{com} w'', \\ B_\omega &= (EI_\omega)_{com} \theta'', \quad M_{sv} = (GJ)_{com} \theta', \end{aligned} \quad (9)$$

where $(EA)_{com}$ denotes axial rigidity. $(EI_y)_{com}$ and $(EI_z)_{com}$ represent the flexural rigidities of the y - and z -axes, respectively. $(EI_\omega)_{com}$ and $(GJ)_{com}$ are, respectively, warping and torsional rigidities of composite thin-walled beams with doubly symmetric I-section, defined by [6, 7]:

$$\begin{aligned} (EA)_{com} &= 2bA_{11}^f + dA_{11}^w, \quad (EI_z)_{com} = \frac{b^3}{6} A_{11}^f + dD_{11}^w, \\ (EI_y)_{com} &= 2bD_{11}^f + \frac{d^2}{2} bA_{11}^f + \frac{d^3}{12} A_{11}^w, \\ (EI_\omega)_{com} &= \left(\frac{d^2}{4} A_{11}^f + D_{11}^f \right) \frac{b^3}{6} + \frac{d^3}{12} D_{11}^w, \\ (GJ)_{com} &= 8bD_{66}^f + 2dD_{66}^w. \end{aligned} \quad (10)$$

That indexes f and w refer to the web and the flange of the beam cross-section, respectively. A_{ij} and D_{ij} are the matrices of extensional and bending stiffness, respectively, which are calculated as

$$\begin{aligned} (A_{ij}^f, D_{ij}^f) &= \sum_{k=1}^N \int_{z_k}^{z_{k+1}} (Q_{ij}^f)_k(1, z^2) dz, \\ (A_{ij}^w, D_{ij}^w) &= \sum_{k=1}^N \int_{y_k}^{y_{k+1}} (Q_{ij}^w)_k(1, y^2) dy, \quad (i = j = 1, 6) \end{aligned} \quad (11)$$

where Q_{ij}^f and Q_{ij}^w are the transformed reduced stiffness related to the flanges and web, respectively. The configuration of lamination is shown in Fig. 2.

Substituting Eq. (9) into Eq. (8), the final form of the variation of the strain energy can be written as following:

$$\delta U_l = \int_L \left((EA)_{com} u'_0 \delta u'_0 + (EI_z)_{com} v'' \delta v'' + (EI_y)_{com} w'' \delta w'' + (EI_\omega)_{com} \theta'' \delta \theta'' + (GJ)_{com} \theta' \delta \theta' \right) dx. \quad (12)$$

Also, the variation form of strain energy due to initial stresses can be stated as:

$$\begin{aligned} \delta U_0 &= \int_V \sigma_{ij}^0 \delta \epsilon_{ij}^* dV = \int_0^L \int_A \sigma_{xx}^0 \delta \epsilon_{xx}^* dA dx \\ &+ 2 \int_0^L \int_A \sigma_{xy}^0 \delta \epsilon_{xy}^* dA dx + 2 \int_0^L \int_A \sigma_{xz}^0 \delta \epsilon_{xz}^* dA dx. \end{aligned} \quad (13)$$

In Eq. (13), σ_{xy}^0 and σ_{xz}^0 indicate the mean values of the shear stress and σ_{xx}^0 signifies initial normal stress in the cross-section. According to Fig. 1, it is contemplated that the external bending moment occurs about the major principal axis (M_y^*). Therefore, the magnitude of bending moment with respect to z -axis is equal to zero. Regarding this, the most general case of normal and shear stresses associated the external bending moment M_y^* and shear force V_z are considered as:

$$\sigma_{xx}^0 = -\frac{M_y^*}{I_y} z, \quad \sigma_{xz}^0 = \frac{V_z}{A} = -\frac{M_y^{*'}}{A}, \quad \sigma_{xy}^0 = 0. \quad (14)$$

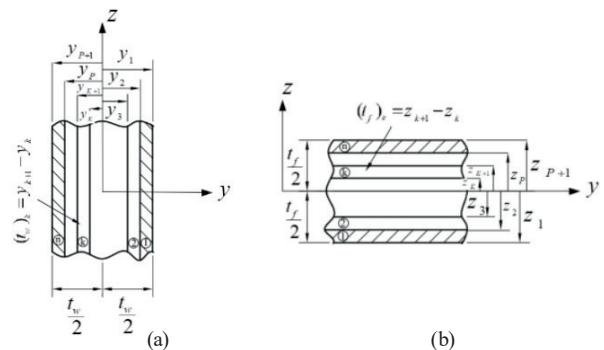


Fig. 2 Web and flanges laminate configuration: (a) FML composite web, (b) FML composite flanges

Substituting Eqs. (3) and (14) into relation Eq. (13), the final form of the variation of strain energy due to the initial stresses is expressed as [22]

$$\delta U_0 = \int_0^L (-M_y^* v'' \delta \theta - M_y^* \theta \delta v'') dx. \quad (15)$$

The first variation of external load work (W_e) of the beam under distributed vertical forces q_z applied along a line (PP') on the section contour (Fig. 1) can be written in the form of

$$\delta W_e = \int_0^L q_z \delta w_p dx. \quad (16)$$

In Eq. (16), w_p is the vertical displacement of point P . According to kinematics used in Asgarian et al. [23], the external work due to transverse loading is defined as

$$\delta W_e = \int_0^L (q_z \delta w - q_z z_p \theta \delta \theta) dx. \quad (17)$$

Here, z_p is used to imply the eccentricity of the applied loads from the centroid of the cross-section. After inserting Eqs. (12), (15) and (17) in Eq. (4), the expression of the first variation of total potential energy can be written as

$$\begin{aligned} \delta \Pi = \int_L & \left((EA)_{com} u_0' \delta u_0' + (EI_z)_{com} v'' \delta v'' \right. \\ & \left. + (EI_y)_{com} w'' \delta w'' \right. \\ & \left. + (EI_\omega)_{com} \theta'' \delta \theta'' + (GJ)_{com} \theta' \delta \theta' \right) dx \\ & + \int_0^L (-M_y^* v'' \delta \theta - M_y^* \theta \delta v'') dx \\ & - \int_0^L (q_z \delta w - q_z z_p \theta \delta \theta) dx = 0, \end{aligned} \quad (18)$$

or equivalently

$$\int_L ((EA)_{com} u_0' \delta u_0') dx = 0, \quad (19)$$

$$\int_L ((EI_y)_{com} w'' \delta w'' - q_z \delta w) dx = 0, \quad (20)$$

$$\int_L ((EI_z)_{com} v'' - M_y^* \theta) \delta v'' dx = 0, \quad (21)$$

$$\int_L \left((EI_\omega)_{com} \theta'' \delta \theta'' + (GJ)_{com} \theta' \delta \theta' - M_y^* v'' \delta \theta + z_p q_z \theta \delta \theta \right) dx = 0. \quad (22)$$

In these equations, the first and second ones are uncoupled and stable, and they do not affect the lateral buckling behavior of FML I-beam subjected to transverse loading. The equilibrium Eqs. (19) and (20) have a coupled nature due to the presence of the lateral deflection v and torsion component θ . Based on the straightforward methodology presented by Soltani et al. [22], Asgarian et al. [23] and Soltani et al. [24], Eq. (21) can be rewritten in the following form for any acceptable lateral buckled configuration:

$$v'' = \frac{M_y^*}{(EI_z)_{com}} \theta, \quad (23)$$

whose substitution in Eq. (22) enables its redefinition in an uncoupled form just dependent on the twist angle θ , independently from the lateral displacement v , i.e.,

$$\int_L \left((EI_\omega)_{com} \theta'' \delta \theta'' + (GJ)_{com} \theta' \delta \theta' - \frac{M_y^{*2}}{(EI_z)_{com}} \theta \delta \theta + z_p q_z \theta \delta \theta \right) dx = 0. \quad (24)$$

In the current study, we use the finite element method for linear lateral-torsional stability analysis of thin-walled FML I-shaped beams with varying web and/or flanges, whose details are presented in the next part.

3 Finite element formulation

According to the authors' knowledge, the lateral-torsional stability behavior of doubly-symmetric thin-walled composite beams with symmetric laminations under bending moment about the strong principal axis of the cross-section is usually governed by two fourth-order differential equations coupled in terms of the lateral displacement and the torsion angle [6, 7]. Accordingly, the 8*8 static and buckling stiffness matrices are formulated based on eight displacement parameters, namely: lateral translation, twist, rotation, and warping at each end node. Whereas in the current finite element model, there are two nodes with two degrees of freedom per node for each element [22]. The two nodes by which the element can be assembled into structure are located at its ends.

According to finite element rules, it is also essential to use local coordinate ($\varepsilon = x/L_e$). L_e is the length of each segment. The local e-axis is directed from node 1 to node 2. The considered degrees of freedom at the left and right nodes of each element are: θ^1, θ^2 (the twist angle), and θ'^1, θ'^2 (the rate of change twist, $\partial\theta/\partial\varepsilon$) [22]. The nodal displacements of the beam element in the local coordinate at $\varepsilon = 0$ and $\varepsilon = 1$ are illustrated in Fig. 3. Within the frame of finite

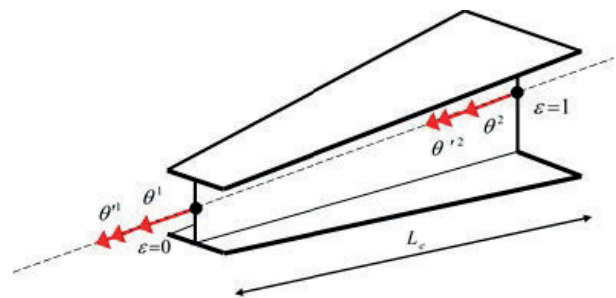


Fig. 3 The nodal displacements of a thin-walled beam

element methodology, the general displacement fields of the considered element with length L_e in the local coordinate can be expressed in terms of nodal degrees of freedom and shape functions for each displacement parameter as

$$\theta(\varepsilon) = [N] \{D\}. \quad (25)$$

In Eq. (25), $\{N\}$ is the vector of shape functions for the twist angle and $\{D\}$ is the vector of nodal degrees of freedom as pictured in Fig. 3, which are described by Eq. (26):

$$\begin{aligned} \{D\} &= \{\theta^1 \quad \theta'^1 \quad \theta^2 \quad \theta'^2\}^T, \\ [N] &= [N_1 \quad N_2 \quad N_3 \quad N_4], \end{aligned} \quad (26)$$

where $N_i, i = 1,2,3,4$ are the shape functions for the four degrees of freedom and commonly called the cubic Hermitian interpolation functions, which are defined by [22]:

$$\begin{aligned} N_1 &= 2\varepsilon^3 - 3\varepsilon^2 + 1, \quad N_2 = \varepsilon^3 - 2\varepsilon^2 + \varepsilon, \\ N_3 &= 2\varepsilon^3 - 3\varepsilon^2 + 1, \quad N_4 = \varepsilon^3 - \varepsilon^2. \end{aligned} \quad (27)$$

Substituting the interpolation shape functions (Eq. (27)) into Eq. (24), the terms of elastic and buckling stiffness matrices of FML tapered beam with doubly symmetric I-section in the non-dimensional coordinate are derived as:

$$\begin{aligned} [K^*] &= \frac{1}{L_e^3} \int_0^1 (EI_\omega)_{com} \{N''\} \{N''\}^T d\varepsilon \\ &\quad + \frac{1}{L_e} \int_0^1 (GJ)_{com} \{N'\} \{N'\}^T d\varepsilon, \\ [K_G] &= \frac{1}{L_e} \int_0^1 \frac{M_y^{*2}}{(EI_z)_{com}} \{N\} \{N\}^T d\varepsilon \\ &\quad - \frac{1}{L_e} \int_0^1 q_z z_p \{N\} \{N\}^T d\varepsilon, \end{aligned} \quad (28)$$

where $[K^*]$ and $[K_G]$ are respectively the usual elastic stiffness and the buckling stiffness matrices. It is necessary to note that in the context of stability analysis, the buckling stiffness matrix is proportional to the initial stress forces.

Based on the finite element instructions and constructing the total stiffness matrices of considered member, the following relation are finally obtained:

$$([K^*] - \lambda [K_G]) \{\Delta\} = \{0\}. \quad (30)$$

In which λ are the eigenvalues and $\{\Delta\}$ are the related eigenvectors. After implementation of the boundary conditions at two ends, not only the lateral buckling loads are computed from the eigenvalue solutions of Eq. (30), but also the twist angle of tapered thin-walled FML beam can be determined.

4 Results and discussion

In the preceding section, an efficient finite element technique has been formulated to calculate the lateral-torsional buckling loads of thin-walled fiber metal laminates beam with varying I-section. In this section, a comprehensive example is conducted to show the effects of significant parameters such as lay-up arrangement, fiber alignment, metal volume fraction, loading position, and web tapering ratio on the lateral buckling capacity of multi-layered composite tapered I-beam. In this regard, the linear lateral buckling analysis is performed for a fixed-free 16-layer FML web tapered I-beam with a span of 5 m under uniformly distributed load. All section walls (both flanges and web) are laminated symmetrically concerning its mid-plane and made of Aluminum alloy 2024-T3 (outer metal layers) and E-glass/epoxy material (fourteen inner composite layers). The material features of the lamina are as follows [18]: for the aluminum plies, $E = 72.4$ GPa and $\nu = 0.33$; and for the fiber-reinforced composite layers, $E_x = 38.6$ GPa, $E_y = 8.27$ GPa, $G_{xy} = 4.14$ GPa, and $\nu_{xy} = 0.26$.

As shown in Fig. 4, at the left end section, both flanges are assumed to be 100 mm wide (b_f), and the web of the I-shape is 300 mm deep (d_L). It is also supposed that the web height of the I-section at the left end (d_L) is made to diminish linearly to (d_R) at the right one. Therefore, the web tapering ratio is defined as $\alpha = d_R/d_L$. Note that this parameter (α) is a non-negative variable and can change from 0.1 to 1.0. Moreover, I-beam with a uniform cross-section is achieved when the mentioned parameter (α) equals one.

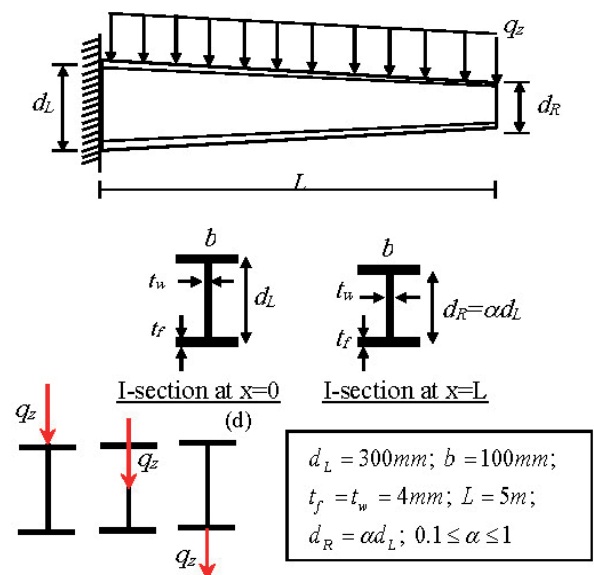


Fig. 4 Cantilever FML I-beam with varying cross-section subjected to uniformly distributed load: Geometrical properties and loading position

In this benchmark example, it is also supposed that uniformly transverse load is applied at three different positions: the top flange, the centroid (shear center), and the bottom flange. It is noteworthy that, to ensure that the lateral buckling mode is overall and there is no local buckling of the flanges and the web, the width-to-thickness ratio for all section walls was checked.

The next part is divided into two different subsections; the first one for checking the convergence and verification of the formulation proposed herein, and the latter aims to peruse the influence of the above-mentioned factors on the linear lateral buckling behavior of the considered member.

4.1 Verification

The aim of the first section of the current example is to define the needed number of segments along the longitudinal direction while using the finite element methodology proposed herein, to obtain the converged results. To this target, the lowest values of the lateral buckling load of the contemplated thin-walled FML profile ($MVF = 0.2$) with variable I-section for two different loading positions and various values of tapering ratios ($\alpha = 0.5, 0.8$ and 1.0) by considering the stacking sequence of $[A1, (0)_7]_s$ for all section walls, are evaluated versus the number of meshes adopted in FE methodology and the outcomes are presented in Fig. 5. It is seen from Fig. 5 that by increasing the number of elements (n) from 6 to 8, the predicted lateral buckling load converges. In the following computations, we take $n = 10$ to calculate the first lateral buckling loads, unless otherwise stated.

In the next step, the lowest values of the lateral buckling loads of the selected tapered FML I-beam with $MVF = 0.45$ for top flange loading, various values of tapering ratios ($\alpha = 0.2, 0.4, 0.6, 0.8$ and 1.0) and two different lay-up arrangements are evaluated and tabulated in Table 1. The accuracy and exactness of the predicted results by the formulation presented herein are checked with those acquired via finite element method (FEM) using commercial software package ANSYS. Additionally, the relative errors (Δ) associated with present approach are presented in Table 1.

Based on the available literature [13–16], SHELL281 is generally adopted to develop FML thin-walled profile using ANSYS, and the lateral-torsional buckling load is estimated by the eigenvalue buckling analysis. SHELL281 has eight nodes with six degrees of freedom at each node: translations in the $x, y,$ and z axes, and rotations about the $x, y,$ and z -axes [26]. In all simulated ANSYS models,

the applied aspect ratio of the mesh (length-to-maximum width) was close to unity at the bigger cross-section. Therefore, the size of meshes is approximately equal to 5 mm in length (Fig. 6). In this example, the boundary condition at the left end is fixed support. Therefore, all displacements and rotations of the end cross-section are restrained and fixed.

As shown in Table 1, the efficiency and performance of the proposed finite element solution are thus confirmed. Fig. 7 shows the overall lateral-torsional buckling mode shape of two of the considered stacking sequences. In the FEM models, local buckling of the web and both flanges is not observed.

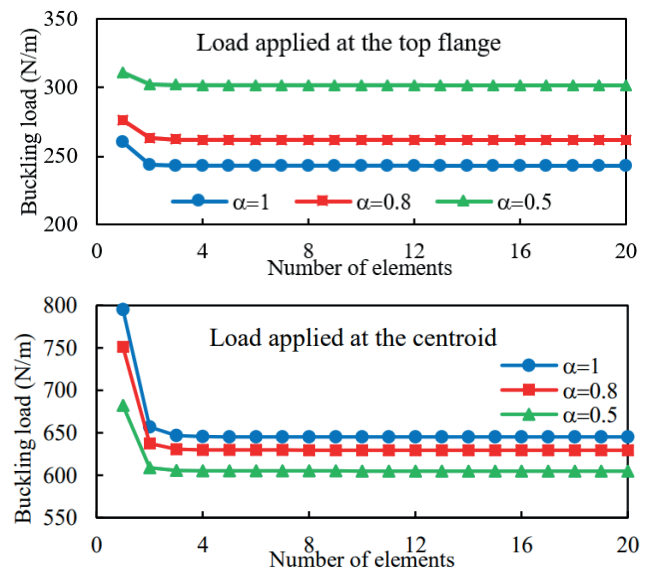


Fig. 5 Estimated lateral buckling load of a fixed-free tapered FML I-section ($[A1, (0)_7]_s$) beam vs. Number of elements

Table 1 The lateral buckling loads comparison between the present methodology and ANSYS for distributed load applied at the top flange when $MVF = 0.45$

Stacking sequence	α	Proposed solution	ANSYS	Δ (%)
$[A1, (0)_7]_s$	0.2	478.139	472.840	1.121
	0.4	427.550	405.770	5.368
	0.6	387.719	357.240	8.532
	0.8	356.590	326.930	9.072
	1	331.972	309.470	7.271
$[A1, (90)_7]_s$	0.2	385.898	377.580	2.155
	0.4	351.903	335.960	4.530
	0.6	323.908	303.150	6.409
	0.8	301.185	280.220	6.961
	1	282.679	265.280	6.155

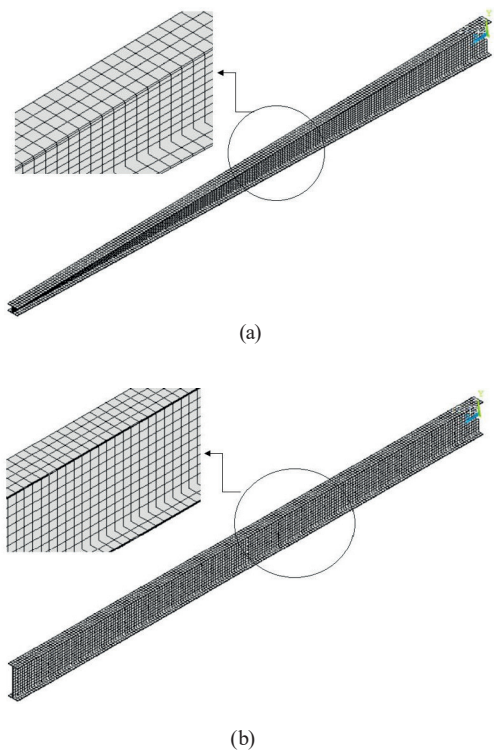


Fig. 6 View of mapped mesh used for the selected member using ANSYS: (a) Web-tapered beam ($\alpha = 0.2$), (b) Prismatic beam ($\alpha = 1$)

4.2 Parametric study

After validating and verifying the methodology proposed herein, the impact of metal volume fraction on lateral stability capacity will be assessed in the following section. The main objective of the next part is also to find out the lay-up arrangement of the inner composite layers of cantilever FML web-tapered I-beam under uniformly distributed load that gives the highest lateral-torsional buckling resistance. In this regard, three different layer sequences are considered.

The first case is that the web and flanges plates are made of 16 plies, including two aluminum sheets and fourteen E-glass/epoxy internal layers, with unidirectional $[Al,(0)_7]_S$ lay-up for the web, while the top and bottom flanges are assumed to have balanced and symmetrical lay-ups $[Al,(0)_7]_S$. For this case, the influence of metal volume fraction on the variations of the lateral buckling load (q_{cr}) of the laminated web-tapered thin-walled beam with $\alpha = 0.4$ related to fiber angle of its flanges (varying from 0 to 90) is plotted in Fig. 8 for the two different loading positions. Load position of uniformly transverse load is on the top flange and mid-height. It is observed from the figures that the endurable lateral buckling load diminishes gradually with an increment in the lamina orientation (θ), where the impact of fiber angle is more perceptible when θ varies in the range of 0 to 60.

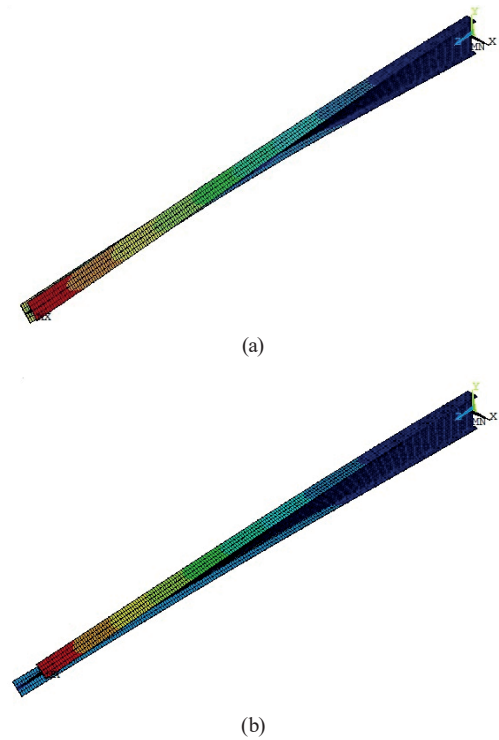


Fig. 7 The FEM result using ANSYS for the first lateral-torsional buckling mode shape: (a) Web-tapered beam ($\alpha = 0.2$) with $[Al,(0)_7]_S$ lamination, (b) Prismatic beam ($\alpha = 1$) with $[Al,(90)_7]_S$ lamination

It can be stated that in the first lateral-torsional buckling mode, the thin-walled FML beam becomes weaker and less stable as the fiber angle increases. The greatest resistance to lateral-torsional buckling is thus obtained with unidirectional $[Al,(0)_7]_S$ lay-up for both flanges.

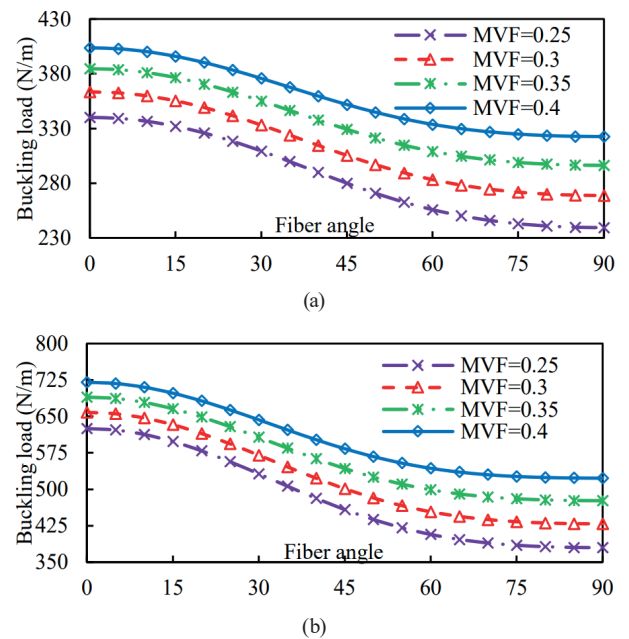


Fig. 8 Variation of the lateral buckling load versus lamina orientation of both flanges for different metal volume fractions: (a) Top flange loading, (b) Centroid loading

In the second case, it is assumed that all section walls (both flanges and the web) are made of fourteen internal layers of E-glass/epoxy and two outer plies of aluminum. The discrepancy between the first two cases is that the fiber of glass/epoxy layers is aligned at zero-degree between the two aluminum sheets in the top and bottom flanges ($[Al(0)_7]_s$), while symmetric angle-ply lay-up arrangement ($[Al(\pm\theta)]_7$) is used in the web. To examine the influence of fiber orientation in the web of FML doubly-symmetric I-section, the fiber angle of each inner ply in the FML hybrid composite web plate is changed with a step of five degrees in the range of $0 \leq \theta \leq 90$. In this case, Fig. 9 exhibits the effect of metal volume fraction (MVF) on the variation of the lateral buckling loads of sandwich fiber-metal laminated web-tapered I-beam related to fiber angle change (θ). The effect of load height position from the cross-section centroid on the lateral buckling resistance is also considered. According to these diagrams, for all values of metal volume percentage, it can be concluded that as the fiber angle is rotated off-axis, the lateral buckling capacity is maximized at $\theta = 45^\circ$ and then minimized sharply at $\theta = 90^\circ$. The highest lateral stability capacity for I-beam is thus obtained by aligning the fiber orientation in the web around 45° . Besides, the lateral buckling behavior is very similar for the two different loading positions.

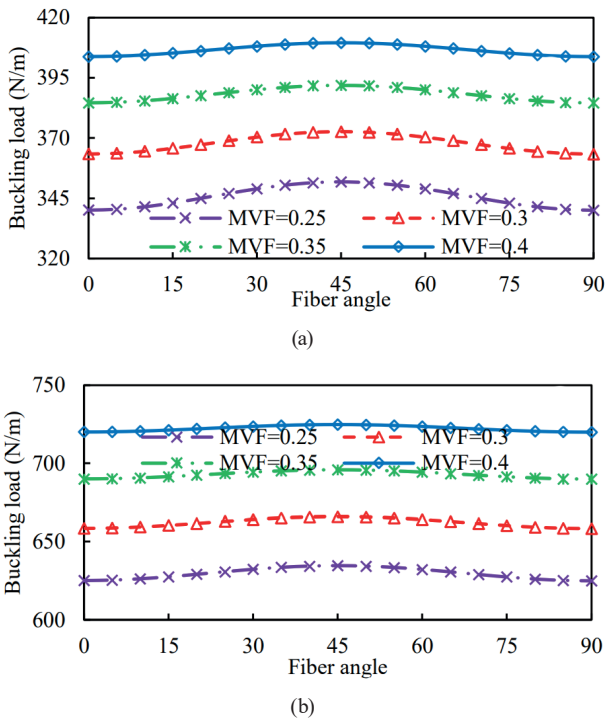


Fig. 9 Variation of the lateral buckling load versus lamina orientation of the web for different metal volume fractions: (a) Top flange loading, (b) Centroid loading

In the third case, it is again assumed that both flanges and web of FML profile with I-section composed of sixteen layers consist of two aluminum sheets and fourteen layers of E-glass/epoxy. The fiber layers in all section walls are placed with the symmetrical and balanced arrangement between the two metal sheets ($[Al(\pm\theta)]_7$). The impact of changing the volume fraction of aluminum and the fiber alignment on the lateral buckling behavior of web-tapered thin-walled tapered beam ($\alpha = 0.4$) for various MVFs (MVF = 0.25, 0.3, 0.35 and 0.4) and considering two different loading positions are presented in Fig. 10. The distributed transverse load can be applied on the top flange, and the centroid.

As can be seen in Fig. 10, the lateral stability decreases steadily as the lamina orientation increases. Besides, this decrease is more pronounced when the fiber angle changes in the range of $0 \leq \theta \leq 60$.

Based on the results presented in Figs. 8–10, we conclude that the endurable lateral buckling increases significantly with increasing the volume fraction of the metal. This result is predictable based on the material properties of E-glass/epoxy and aluminum. Also, according to these illustrations, it can be stated that as the percentage of aluminum increases, the effect of the lamina orientation on the lateral stability of the FML web-tapered I-beam decreases significantly. This consequence is due to thickening aluminum sheets and thinning fiber-reinforced epoxy composite layers.

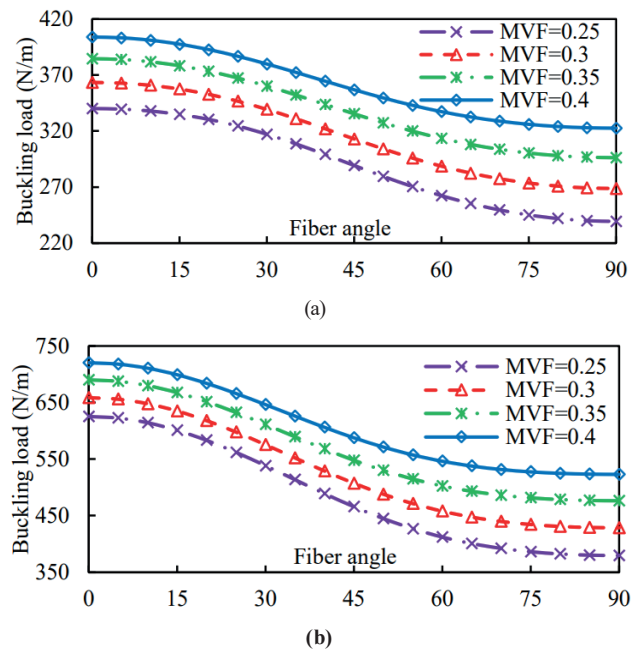


Fig. 10 Variation of the lateral buckling load versus lamina orientation of the web and both flanges for different metal volume fractions: (a) Top flange loading, (b) Centroid loading

Based on the results presented in Figs. 8–10, it can be concluded that the optimum fiber angles for achieving the highest lateral buckling resistance of cantilever FML web tapered beam under distributed load are $\pm 45^\circ$ in the web and 0° both flanges. This statement is reasonable since the flexural stiffness $(EI)_{z,com}$ and the warping rigidity $(EI)_{\omega,com}$ are expressed in unidirectional stiffness A_{11} and D_{11} (Eq. (10)). These two components achieve their maximum magnitude by aligning the constituent fibers of the web and both flanges at zero along the beam length. Since the flanges should resist most bending and warping moments and the two above stiffness quantities $((EI)_{z,com}$ and $(EI)_{\omega,com}$) are typically controlled by the fiber angle in the top and bottom flanges; hence the fiber orientation should be placed 0° in both flanges to increase the lateral-torsional stability capacity. Based on Eq. (10), the laminate torsional stiffness $(GJ)_{com}$ is presented in twisting stiffness of both flanges D_{66}^f and the web D_{66}^w . These two parameters usually reach their maximum value by placing the fibers of the composite layers along 45° . Since the web of the I-section withstands shear stresses and has to transmit vertical shear force, the web fiber must be placed at an angle of $\pm 45^\circ$ to achieve the maximum shear capacity for the cross-section.

Considering the optimal stacking sequence, the magnitude of lateral-torsional buckling loads for various combinations of web tapering ratio and MVFs, with different loading positions are listed in Table 2.

Table 2 shows that the web non-uniformity parameter has a considerable impact on the endurable lateral-torsional buckling load. The tapering parameter weakens the

beam loaded on the shear center and bottom flange due to decreasing the member stiffness, while the other results relating to cantilever web tapered I-beams under top flange loading do not follow the same trajectory. This may indicate that the lateral stability resistance corresponding to the top is enhanced with tapering ratio. For instance, the lateral buckling loads of FML cantilevers with constant cross-section are smaller than those of web-tapered with tapering ratio equal to 0.4. This interesting reason is attributed to the fact that the torsion moment due to lateral load height $(q_z z_p)$ is decreased by descending the taper ratio (α) from 1. Finally, it can be stated that this phenomenon

Table 2 Lateral buckling load for FML tapered I-beam with different tapering ratios, metal volume fractions and loading position

Loading position	α	Metal volume fraction				
		0	0.2	0.4	0.6	0.8
Top flange	1	161.217	259.223	324.219	368.458	398.722
	0.8	173.116	278.207	347.765	395.659	428.994
	0.6	188.948	302.467	377.508	430.052	467.519
	0.4	210.972	334.032	415.540	474.062	517.243
Centroid	1	493.217	659.840	793.056	907.721	1009.834
	0.8	480.239	643.463	773.723	885.755	985.495
	0.6	466.594	626.398	753.625	862.908	960.132
	0.4	452.146	608.539	732.660	839.056	933.585
Bottom flange	1	860.062	1069.447	1265.684	1452.685	1633.506
	0.8	811.449	1011.493	1197.912	1374.807	1545.332
	0.6	759.799	950.232	1126.372	1292.586	1452.166
	0.4	703.924	884.497	1049.775	1204.534	1352.263

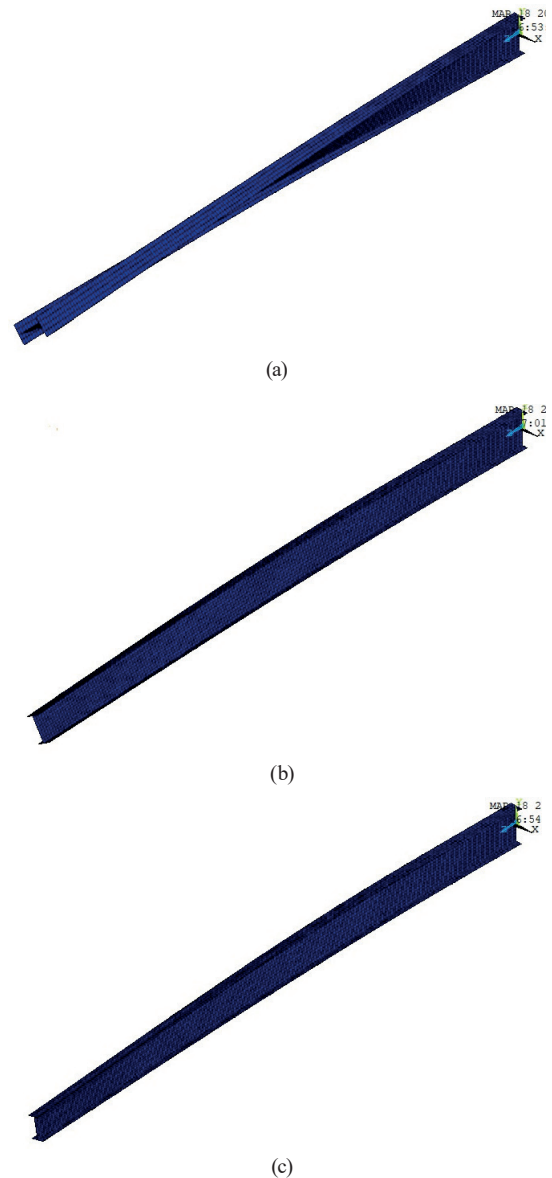


Fig. 11 The FEM result using ANSYS for the three first lateral-torsional buckling mode shapes for web-tapered beam ($\alpha = 0.6$) with MVF = 0.4: (a) Top flange loading, (b) Centroid loading, (c) Bottom flange loading

is more predominant on lateral buckling resistance of cantilever beam subjected to transverse load than that of web non-uniformity ratio. Because of space limitations, only the first three lateral buckling modes of cantilever FML web-tapered beam ($\alpha = 0.6$) with MVF = 0.4 having the best stacking sequences is depicted in Fig. 11. As shown in this figure, the influence of active and passive torsional moments due to the transverse load height parameter is respectively observed for the loading cases on the top and bottom flanges. Again, no local buckling of both flanges and the web is observed for three loading positions.

5 Conclusions

Lateral buckling of sandwich fiber-metal laminate tapered I-beams subjected to transverse loading has been investigated in the present work by the finite element approach. It is assumed that all section walls (the web and both flanges) are laminated symmetrically concerning its mid-plane and consist of two metal layers at the outer sides of fiber-reinforced epoxy composite laminates. To derive the total potential energy, Vlasov's theory of open thin-walled beams in conjugate with the classic lamination theory is employed. The effect of load position on the lateral stability strength of the beam is also included in the formulation. Then the weak form expression of the governing equation is constructed in terms of the twist angle using an auxiliary equation. Finally, the structural stiffness matrices are formulated throughout two-node Hermitean finite beam elements with two degrees of freedom per node. The superiority of the proposed approach is to provide a two-node laminated I-beam element with a low number of degrees of freedom. Therefore, the present finite element model can simplify and decrease the essential computational efforts to calculate the lateral buckling load of thin-walled FML beams with varying cross-sections. In this research,

E-glass/epoxy is considered for composite plies and aluminum for metal sheets. After verification with ANSYS software, the influence of fiber angle, stacking sequence, metal volume fraction, transverse loading position, and web tapering ratio on lateral-torsional stability of cantilever composite 16-layer FML tapered I-beam is thoroughly measured. The results of this research can be expressed as:

- For all transverse loading positions, it was found that the lateral buckling parameter of hybrid fiber-metal laminates beam with tapered I-section decreases as the fiber orientation in both flanges is rotated off-axis.
- The maximum lateral buckling load for cantilever FML web tapered I-beam subjected to uniformly distributed load is obtained by placing the fiber angle of each inner composite ply at $\pm 45^\circ$ in the web and 0° in both flanges.
- The results show that increasing the metal volume fraction leads to enhance linear buckling strength of glass-reinforced aluminum laminate I-beam under transverse loading.
- For the optimal layer arrangement, the lateral buckling load increases approximately 30% by raising the metal volume percentage from 0% to 20% when the load is applied at the bottom flange.
- As aluminum volume fraction increases, the effect of changing the fiber angle on the lateral stability of FML web-tapered I-beam under transverse load decreases significantly
- The effect of metal volume fraction (MVF) on the lateral buckling capacity is more than the web tapering parameter.
- It is observed that the buckling capacity of cantilever FML beam with doubly-symmetric I-section is best when the uniformly distributed load is applied on the bottom flange.

References

- [1] Nam, H. W., Hwang, W., Han, K. S. "Stacking sequence design of fiber-metal laminate for maximum strength", *Journal of Composite Materials*, 35(18), pp. 1654–1683, 2001.
<https://doi.org/10.1106/7NV4-5J5R-XIUJ-PVXT>
- [2] Andrade, A., Camotim, D., Dinis, P. B. "Lateral-torsional buckling of singly symmetric web-tapered thin-walled I-beams: 1D model vs. shell FEA", *Computers & Structures*, 85, pp. 1343–1359, 2007.
<https://doi.org/10.1016/j.compstruc.2006.08.079>
- [3] Andrade, A., Camotim, D., e Costa, P. P. "On the evaluation of elastic critical moments in doubly and singly symmetric I-section cantilevers", *Journal of Constructional Steel Research*, 63(7), pp. 894–908, 2007.
<https://doi.org/10.1016/j.jcsr.2006.08.015>
- [4] Mohri, F., Bouzerira, C., Potier-Ferry, M. "Lateral buckling of thin-walled beam-column elements under combined axial and bending loads", *Thin-Walled Structures*, 46(3), pp. 290–302, 2008.
<https://doi.org/10.1016/j.tws.2007.07.017>
- [5] Ravishankar, H., Rengarajan, R., Devarajan, K., Kaimal, B. "Free vibration behaviour of fiber metal laminates, hybrid composites, and functionally graded beams using finite element analysis", *International Journal of Acoustics and Vibration*, 21(4), pp. 418–428, 2016.
<https://doi.org/10.20855/ijav.2016.21.4436>
- [6] Lee, J., Kim, S.-E., Hong, K. "Lateral buckling of I-section composite beams", *Engineering Structures*, 24(7), pp. 955–964, 2002.
[https://doi.org/10.1016/S0141-0296\(02\)00016-0](https://doi.org/10.1016/S0141-0296(02)00016-0)

- [7] Lee, J. "Flexural analysis of thin-walled composite beams using shear-deformable beam theory", *Composite Structures*, 70(2), pp. 212–222, 2005.
<https://doi.org/10.1016/j.compstruct.2004.08.023>
- [8] Lezgy-Nazargah, M. "A generalized layered global-local beam theory for elasto-plastic analysis of thin-walled members", *Thin-Walled Structures*, 115, pp. 48–57, 2017.
<https://doi.org/10.1016/j.tws.2017.02.004>
- [9] Wackerfuß, J., Kroker, A. M. "An efficient semi-analytical simulation framework to analyze laminated prismatic thin-walled beams", *Computers & Structures*, 208, pp. 32–50, 2018.
<https://doi.org/10.1016/j.compstruc.2018.06.010>
- [10] Ahmadi, H., Rasheed, H. A. "Lateral torsional buckling of anisotropic laminated thin-walled simply supported beams subjected to mid-span concentrated load", *Composite Structures*, 185, pp. 348–361, 2018.
<https://doi.org/10.1016/j.compstruct.2017.11.027>
- [11] Asadi, A., Sheikh, A. H., Thomsen, O. T. "Buckling behaviour of thin-walled laminated composite beams having open and closed sections subjected to axial and end moment loading", *Thin-Walled Structures*, 141, pp. 85–96, 2019.
<https://doi.org/10.1016/j.tws.2019.04.005>
- [12] Soltani, M. "Flexural-torsional stability of sandwich tapered I-beams with a functionally graded porous core", *International Journal of Numerical Methods in Civil Engineering*, 4(3), pp. 8–20, 2020.
<https://doi.org/10.52547/nmce.4.3.8>
- [13] Banat, D., Kolakowski, Z., Mania, R. J. "Investigations of FML profile buckling and post-buckling behaviour under axial compression", *Thin-Walled Structures*, 107, pp. 335–344, 2016.
<https://doi.org/10.1016/j.tws.2016.06.018>
- [14] Banat, D., Mania, R. J. "Failure assessment of thin-walled FML profiles during buckling and postbuckling response", *Composites Part B: Engineering*, 112, pp. 278–289, 2017.
<https://doi.org/10.1016/j.compositesb.2017.01.001>
- [15] Banat, D., Mania, R. J. "Progressive failure analysis of thin-walled Fibre Metal Laminate columns subjected to axial compression", *Thin-Walled Structures*, 122, pp. 52–63, 2018.
<https://doi.org/10.1016/j.tws.2017.09.034>
- [16] Banat, D., Mania, R. J. "Stability and strength analysis of thin-walled GLARE composite profiles subjected to axial loading", *Composite Structures*, 212, pp. 338–345, 2019.
<https://doi.org/10.1016/j.compstruct.2019.01.052>
- [17] Secer, M., Uzun, E. T. "Inelastic ultimate load analysis of steel frames considering lateral torsional buckling under distributed loads", *Periodica Polytechnica Civil Engineering*, 63(3), pp. 872–881, 2019.
<https://doi.org/10.3311/PPci.13513>
- [18] Ghasemi, A. R., Mohandes, M. "Comparison between the frequencies of FML and composite cylindrical shells using beam modal function model", *Journal of Computational Applied Mechanics*, 50(2), pp. 239–245, 2019.
<https://doi.org/10.22059/JCAMECH.2019.64657>
- [19] Ghasemi, A. R., Mohandes, M. "Free vibration analysis of micro and nano fiber-metal laminates circular cylindrical shells based on modified couple stress theory", *Mechanics of Advanced Materials and Structures*, 27(1), pp. 43–54, 2020.
<https://doi.org/10.1080/15376494.2018.1472337>
- [20] Ghasemi, A. R., Kiani, S., Tabatabaeian, A. "Buckling analysis of FML cylindrical shells under combined axial and torsional loading", *Mechanics of Advanced Composite Structures*, 7(2), pp. 263–270, 2020.
<https://doi.org/10.22075/MACS.2020.18521.1219>
- [21] Ton-That, H. L., Nguyen-Van, H. "A combined strain element in static, frequency and buckling analyses of laminated composite plates and shells", *Periodica Polytechnica Civil Engineering*, 65(1), pp. 56–71, 2021.
<https://doi.org/10.3311/PPci.16809>
- [22] Soltani, M., Asgarian, B., Mohri, F. "Improved finite element model for lateral stability analysis of axially functionally graded nonprismatic I-beams", *International Journal of Structural Stability and Dynamics*, 19(09), 1950108, 2019.
<https://doi.org/10.1142/S0219455419501086>
- [23] Asgarian, B., Soltani, M., Mohri, F. "Lateral-torsional buckling of tapered thin-walled beams with arbitrary cross-sections", *Thin-Walled Structures*, 62, pp. 96–108, 2013.
<https://doi.org/10.1016/j.tws.2012.06.007>
- [24] Soltani, M., Atoufi, F., Mohri, F., Dimitri, R., Tornabene, F. "Nonlocal elasticity theory for lateral stability analysis of tapered thin-walled nanobeams with axially varying materials", *Thin-Walled Structures*, 159, 107268, 2021.
<https://doi.org/10.1016/j.tws.2020.107268>
- [25] Vlasov, V. Z. "Thin-Walled Elastic Beams", Israel Program for Scientific Translation, Jerusalem, Israel, 1961.
- [26] ANSYS "Version 15.0" [computer program] Swanson Analysis System, Canonsburg, PA, USA, 2007.